Do not remove

PROJECT MATTERHORN

Contract AT(30-1) – 1238 with the
U S Atomic Energy Commission

AEC RESEARCH AND DEVELOPMENT REPORT

PRINCETON UNIVERSITY

PRINCETON, NEW JERSEY

Project Matterhorn
Princeton University
Princeton, N.J.

Doppler Broadening of the He^{+} 4686 Line in Ion Temperature Measurements*

K.E. Weimer

January 1957

Technical Memo No. 42 NYO-7885

AEC Research and Development Report

This work was supported under Contract AT(30-1)-1238 with the Atomic Energy Commission.

---

*Retyped - November 19, 1959

Doppler Broadening of the He^+ 4686 Line in Ion Temperature Measurements

January 1957

Abstract

The measurement of the broadening of the He II complex line λ 4686 A has been widely used [1] to estimate ion temperatures in plasmas. Such broadening has been assumed as a first approximation to arise only from the Doppler effect. This report attempts to analyze the broadening as a function of both temperature and magnetic field. All other sources of broadening have been assumed to be negligible.

Fine Structure of He^+ 4686 A

The line He^+ 4686 arises from a principal series 4 to 3 transition; its fine structure has been analyzed extensively both theoretically and experimentally [2, 3, 4, 5, 6]. Table I gives the transitions involved, the wave numbers (vacuum)[7] and wave lengths (air) together with the calculated and observed relative intensities of the various components. The wave length in air is determined by subtracting 1.311 A, the correction due to the change in the index of refraction, from the vacuum wave length.

Table I Fine Structure of He^+ 4686

	Transition	Vacuum $\gamma(cm^{-1})$	λ(in A^o) air	Sommerfeld Intensity Cal.	G. W. Series Intensity Cal.	G. W. Series (observed)
I	$3^2D_{\frac{3}{2}} - 4^2P_{\frac{1}{2}}$	21334.564	4685.918	1.0	0.63	
I'	$3^2P_{\frac{3}{2}} - 4^2S_{\frac{1}{2}}$	21334.623	4685.905	2.0	2.2	11.3
II	$3^2D_{\frac{5}{2}} - 4^2P_{\frac{3}{2}}$	21334.718	4685.885	0.12	1.14	
III	$3^2D_{\frac{5}{2}} - 4^2F_{\frac{5}{2}}$	21334.961	4685.831	4.6	5.1	100
IV	$3^2D_{\frac{5}{2}} - 4^2F_{\frac{7}{2}}$	21335.083	4685.805	92.3	1.00	
V	$3^2P_{\frac{3}{2}} - 4^2D_{\frac{3}{2}}$	21335.295	4685.758	3.9	4.2	4.84
V'	$3^2D_{\frac{3}{2}} - 4^2P_{\frac{3}{2}}$			0.59	0.12	

Table I Fine Structure of He^+ 4686 (contd.)

	Transition	Vacuum $\gamma(cm^{-1})$	λ(in A^o) air	Sommerfeld Intensity Calc.	G.W. Series Intensity Calc.	G.W. Series (observed)
VI	$3^2P_{\frac{3}{2}} - 4^2D_{\frac{5}{2}}$	21335.538	4685.705	64.6	70.1	106.5
VI'	$3^2D_{\frac{3}{2}} - 4^2F_{\frac{5}{2}}$			35.4	38.3	
VII	$3^2S_{\frac{1}{2}} - 4^2P_{\frac{1}{2}}$	21336.156	4685.569	5.1	5.6	4.8
VII'	$3^2P_{\frac{1}{2}} - 4^2S_{\frac{1}{2}}$	21336.354	4685.525	1.0	1.1	4.8
VIII	$3^2S_{\frac{1}{2}} - 4^2P_{\frac{3}{2}}$	21336.887	4685.408	10.3	11.1	11.3
VIII'	$3^2P_{\frac{1}{2}} - 4^2D_{\frac{3}{2}}$	21337.026	4685.378	19.6	21.3	21.0

Generally, the agreement between the observed and calculated intensities is good. Anomalous intensities[3] were observed for the lines I' and VII', both of which were about five times the calculated value. Since both have the common upper level $S_{\frac{1}{2}}$, a possible explanation was that this level was overpopulated by a factor of five in the discharge. Similar anomalies had been observed by Paschen and Leo. Apparently, the intensities of the two lines are rather sensitive to discharge conditions.

In the calculation of the broadening of the complex line, theoretical values of the intensities only have been used. Only those components whose intensities compared to 100 are at least 5 are here considered. Statistical equilibrium has been assumed to exist among the various upper levels. Experimentally, at sufficiently low pressure, this equilibrium may not always be attained[8] with a consequent increase in intensity of the components originating from the 4P levels.

Doppler Broadening

Doppler broadening has been calculated using the formula for the intensity as a function of temperature and wave length shift

$$I(\lambda) = I_{max} e^{-\frac{m}{2kt} \frac{c^2}{\lambda_o^2} \Delta\lambda^2}$$

where λ_o is the wave length of the unshifted line and $\Delta\lambda$ is the displacement from λ_o. For He^+4686, this becomes

$$I = I_{max} e^{-85.052 \Delta\lambda^2/T}$$

where T is the "temperature" in electron volts (1 ev = 1.16×10^4 ^oK) and $\Delta\lambda$ is in angstroms. The theoretical profiles for the composite line at various temperatures are shown in Figure 1. Half-intensity total widths Γ obtained from these curves as a function of ion temperature are given in Table 2 and plotted in Figure 2.

Table 2. Total Widths (at half-intensity) of He^+ 4686

Ion Temperature (ev)	Γ = Total Width (A)
1	0.22
16	0.77
36	1.11
49	1.29
81	1.63
100	1.80

The broadening due to fine structure is completely masked at temperatures above 80 ev, and a simple formula may be used to determine the Doppler broadening.

$$\Gamma = 0.18\ T^{\frac{1}{2}} \quad \text{(T in ev where 1 ev} = 1.16 \times 10^4\ ^oK.)$$

Zeeman Effect

For the purpose of approximating the effect of the magnetic field on the line profile, the so-called "normal Zeeman effect" has been considered rather than the "anomalous Zeeman effect" which is actually involved and which, if used, would have led to an unnecessarily complicated analysis. For observation perpendicular to the field, normal Zeeman effect gives rise to a central undisplaced π component ($\Delta m = 0$, plane polarized parallel to the field) and to two σ components ($\Delta m = \pm 1$, plane polarized perpendicular to the field) displaced from the central component a distance

$$\Delta\gamma = 4.67 \times 10^{-5} H$$

where $\Delta\gamma$ is in wave numbers and H is in gauss. For $He^{+}4686$ this displacement becomes, in angstroms,

$$\Delta\lambda = 1.012 \times 10^{-5} H$$

Actually, several lines are grouped around the three "normal" positions (anomalous Zeeman effect). The individual displacements are small relative to the normal shift, however, and, for simplicity, are here replaced by a single line of intensity equal to the sum of the individual intensities (the summed intensity of the $\Delta m = +1$ components is approximately one-half that of the total intensity of the undisplaced $\Delta m = 0$ components and similarly for the $\Delta m = -1$ components). For observation along the field, the $\Delta m = 0$ transitions are forbidden; $\Delta m = \pm 1$ are circularly polarized. Wave number and wave length displacements as a function of magnetic field are given in Table 3.

Table 3. Displacement of $\Delta m = \pm 1$ components from $\Delta m = 0$ component

Magnetic Field kilogauss	$\Delta \gamma$ cm^{-1}	$\Delta \lambda$ Angstroms
10	0.467	0.101
20	0.934	0.202
30	1.401	0.303
40	1.868	0.405
50	2.335	0.506

The $\Delta m = 0$ components could be separated by the use of a polarizer, but this procedure would result in a loss of over 50% of the intensity in transverse observation. Composite profiles for the Doppler-broadened Zeeman components for various temperatures have been made and are shown in Figures 3-6 (the a figures refer to transverse observation without polarizer, and the b pictures to longitudinal observation.) Figures 7 (a and b) and 8 (a and b) represent broadening (half-intensity total width Γ) as a function of temperature with magnetic field as a parameter and as a function of magnetic field with temperature as a parameter, respectively, for observation in the two directions. These results are displayed in Tables 4a and 4b. The values obtained at fields of 15000 gauss and higher are the result of approximations to the Paschen-Back effect which occurs in such fields.

Table 4a. Calculated total widths Γ at half-intensity for transverse ($\Delta m = 0, \pm 1$) observation of He^+ 4686 as a function of temperature and magnetic field. No polarizer.

Magnetic Field kilogauss	Temperature 16 ev	36 ev	49 ev	100 ev
0	0.77	1.11	1.29	1.80
10	0.77	1.11	1.29	1.80
30	0.96	1.21	1.38	1.88
50	1.25	1.43	1.58	2.03

Table 4b. Calculated total widths Γ at half-intensity for longitudinal ($\Delta m = \pm 1$) observation of He^+ 4686 as a function of temperature and magnetic field.

Magnetic Field kilogauss	Temperature 4ev	9ev	16ev	25ev	36ev	49ev	64ev	100ev
0	0.43	0.60	0.77	0.94	1.11	1.29	1.46	1.80
10	0.49	0.65	0.81	0.98	1.13	1.31	1.47	1.81
15	0.63	0.73	0.86	1.01	1.17	1.33	1.48	1.82
20	0.79	0.84	0.94	1.07	1.22	1.38	1.52	1.87
30	1.04	1.16	1.20	1.29	1.39	1.52	1.65	1.95
40	1.24	1.39	1.54	1.59	1.64	1.72	1.83	2.10
50	1.44	1.58	1.76	1.89	1.97	2.02	2.10	2.30

Paschen-Back Effect

In the presence of a sufficiently high magnetic field, the spin-orbit interaction may become relatively slight; l-s coupling will no longer be valid and the lines corresponding to the transitions given in Table 1 do not exist as a consequence of the overlapping of the magnetic levels. The spin-orbit interaction energy may be determined from the fine structure shifts, and, in Table 5, this shift is related to a corresponding magnetic field in gauss.

Table 5. Spin-orbit Interaction Energy

Doublet	Separation $\Delta\gamma$ (cm^{-1})	$H = \Delta\gamma/4.669 \times 10^{-5}$ gauss
$3^2P_{\frac{1}{2}}$, $3^2P_{\frac{3}{2}}$	1.731	37000
$3^2D_{\frac{3}{2}}$, $3^2D_{\frac{5}{2}}$	0.577	26900
$4^2P_{\frac{1}{2}}$, $4^2P_{\frac{3}{2}}$	0.731	34100
$4^2D_{\frac{3}{2}}$, $4^2D_{\frac{5}{2}}$	0.243	11300
$4^2F_{\frac{5}{2}}$, $4^2F_{\frac{7}{2}}$	0.122	2600

As the most intense components arise from the 4D and 4F levels, it can be seen from the table that magnetic fields greater than 12000 gauss would give rise to the Paschen-Back effect. Consequently, an estimated Paschen-Back pattern was plotted based on the following:

1. The sum of the intensities of all components for field-free transitions equals the sum of the intensities for field transitions between levels having the same n, l values. For example, the transitions for the Paschen-Back line $3^2D - 4^2F$ have the same summed intensity as the sum of intensities for $3^2D_{\frac{5}{2}} - 4^2F_{\frac{5}{2}}$, $3^2D_{\frac{5}{2}} - 4^2F_{\frac{7}{2}}$, $3^2D_{\frac{3}{2}} - 4^2F_{\frac{5}{2}}$ and similarly for $3^2S - 4^2P$, $3^2P - 4^2S$, etc.

2. The small, individual displacements of the magnetic components are ignored and a single line replaces them. Intensities of the $\Delta m = +1$ and $\Delta m = -1$ components are assumed equal to one half that of the undiplaced $\Delta m = 0$ component as was true for the low field case. Table 6 gives the new transitions together with wave lengths and assigned intensities. These wave lengths and intensities were then used to determine composite profiles. In one instance, T = 36 ev and H = 50,000 gauss, the profile ($\Delta m = 0, \pm 1$) was determined using both Zeeman and Paschen-Back transitions. The results were nearly identical. ($\Gamma = 1.43$ and 1.45, respectively)

Table 6. Paschen-Back Transitions

Transition	λ	Intensity	
$3^2S - 4^2P$	4685.46	11.6	
$3^2P - 4^2D$	4685.60	66.7	064 009
$3^2D - 4^2F$	4685.77	1.00	
$3^2P - 4^2S$	4685.78	2.3	(neglected)
$3^2D - 4^2P$	4685.89	1.3	(neglected)

Effect of Slit Width

A check was made on the "averaging" effect resulting from 0.1 A and 0.2 A experimental resolution for scans made at 0.1 A intervals. The error introduced at these resolutions is significant only at low temperatures where the line still shows structure. For example, at T = 1 ev, resolution 0.2 A, the "observed" half-width expected was 0.28 A compared to a theoretical value of 0.22 A (error 27%). However, at 16 ev, resolution 0.2 A, the error was less than 1%, well within the experimental error.

Addendum

Low Temperature Profiles Viewed along the Magnetic Field

At low ion temperatures, He^{+}4686 shows definite structure when viewed in a direction parallel ($\Delta m = \pm 1$) to the magnetic field for ($H \geq 20,000$ gauss). Two profiles, indicative of the behavior to be expected for ion temperatures of 4 and 9 ev (Figures 9 and 10, respectively) have consequently been included. Paschen-Back transitions were used and "broadenings" have been tabulated on the figures.

References

1. S.P. Cunningham, WASH-289, 279-287 (1955)
TID-7503, 19-25 (1955)
TID-7520 (Part 2), 470-479 (1956)

2. F. Paschen, Ann. Phys. 82, 692 (1927)

3. A. Sommerfeld and A. Unsöld, Z Phys. 38, 237 (1926)

4. G.W. Series, Proc. Roy. Soc. (London), A 226, 377-392 (1954). The Fine Structure of the Line 4686 Å of Singly Ionized Helium.

5. G. Herzberg, Z Phys. 146, 269-280 (1956), The Fine Structure of the He^+ Lines 1640 A^o and 4686 A^o.

6. P.S. Kireev, Soviet Doklady 1 (1), 74-76 (1956)
Dokl. Akad. Nauk SSSR 106, (4) 630-633 Relative Intensity of the Fine Structure Components of He II 4686 A^o.

7. Charlotte Moore, Atomic Energy Levels 1949, NBS Circular 467.

8. S.P. Cunningham, TID-7520 (Part 2), 470-479 (1956)
Spectroscopic Determination of Ion Temperatures.

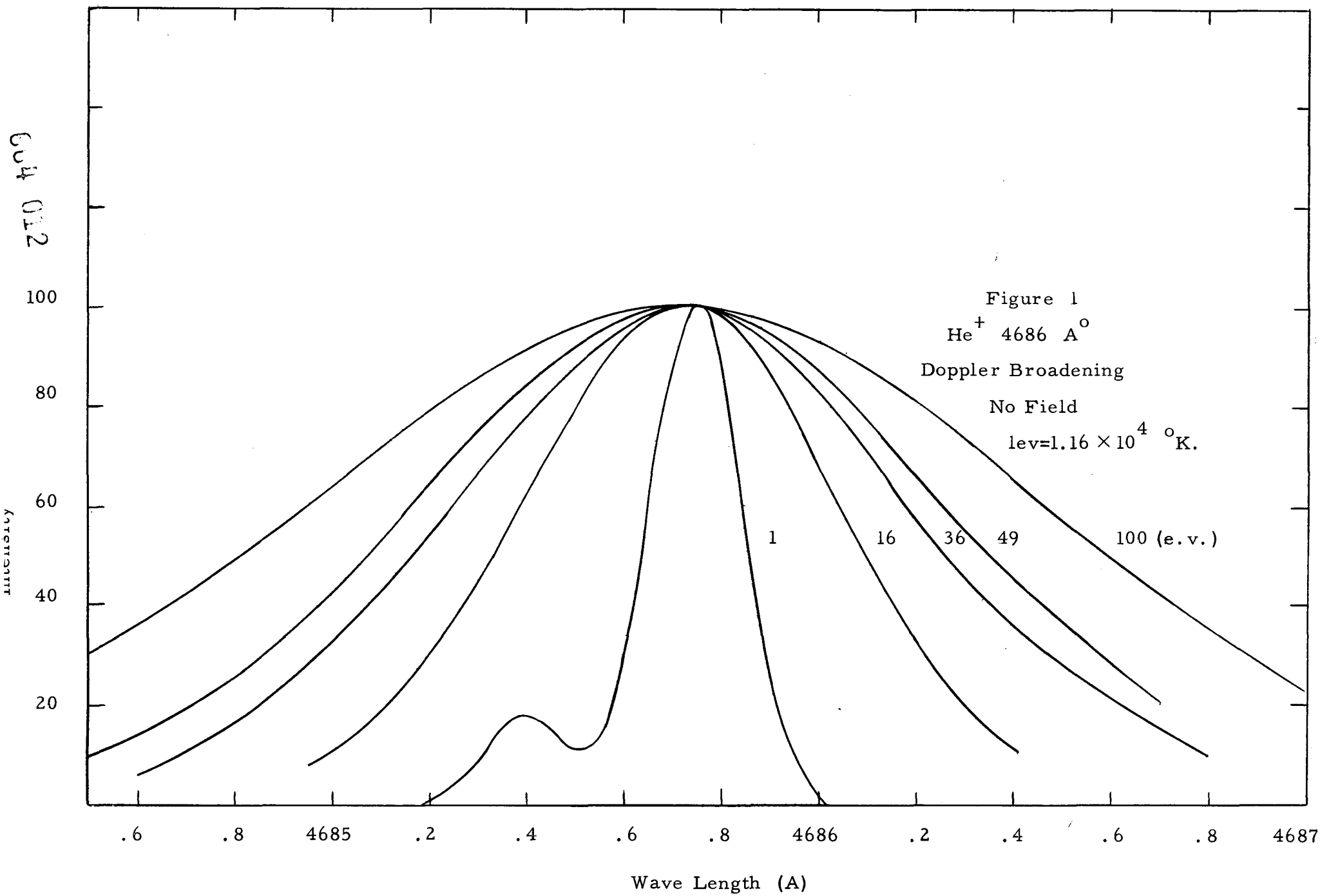
Cyh 012
100
80
60
40
20
Intensity
Figure 1
He+ 4686 A°
Doppler Broadening
No Field
1ev=1.16 × 10^4 °K.
1
16
36
49
100 (e.v.)
.6
.8
4685
.2
.4
.6
.8
4686
.2
.4
.6
.8
4687
Wave Length (A)

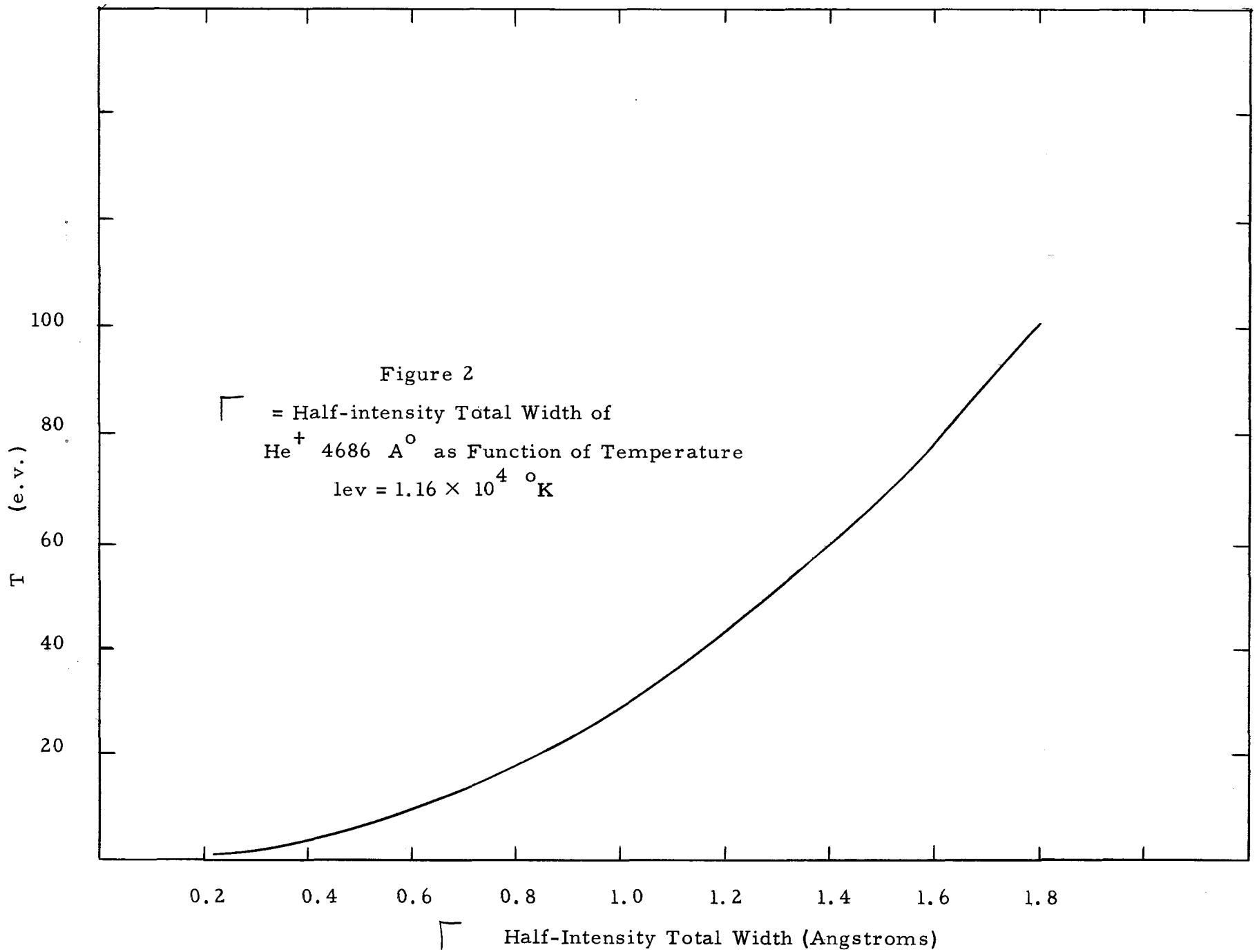

Figure 2

Γ = Half-intensity Total Width of

He^{+} 4686 A^{o} as Function of Temperature

lev = 1.16×10^{4} ^{o}K

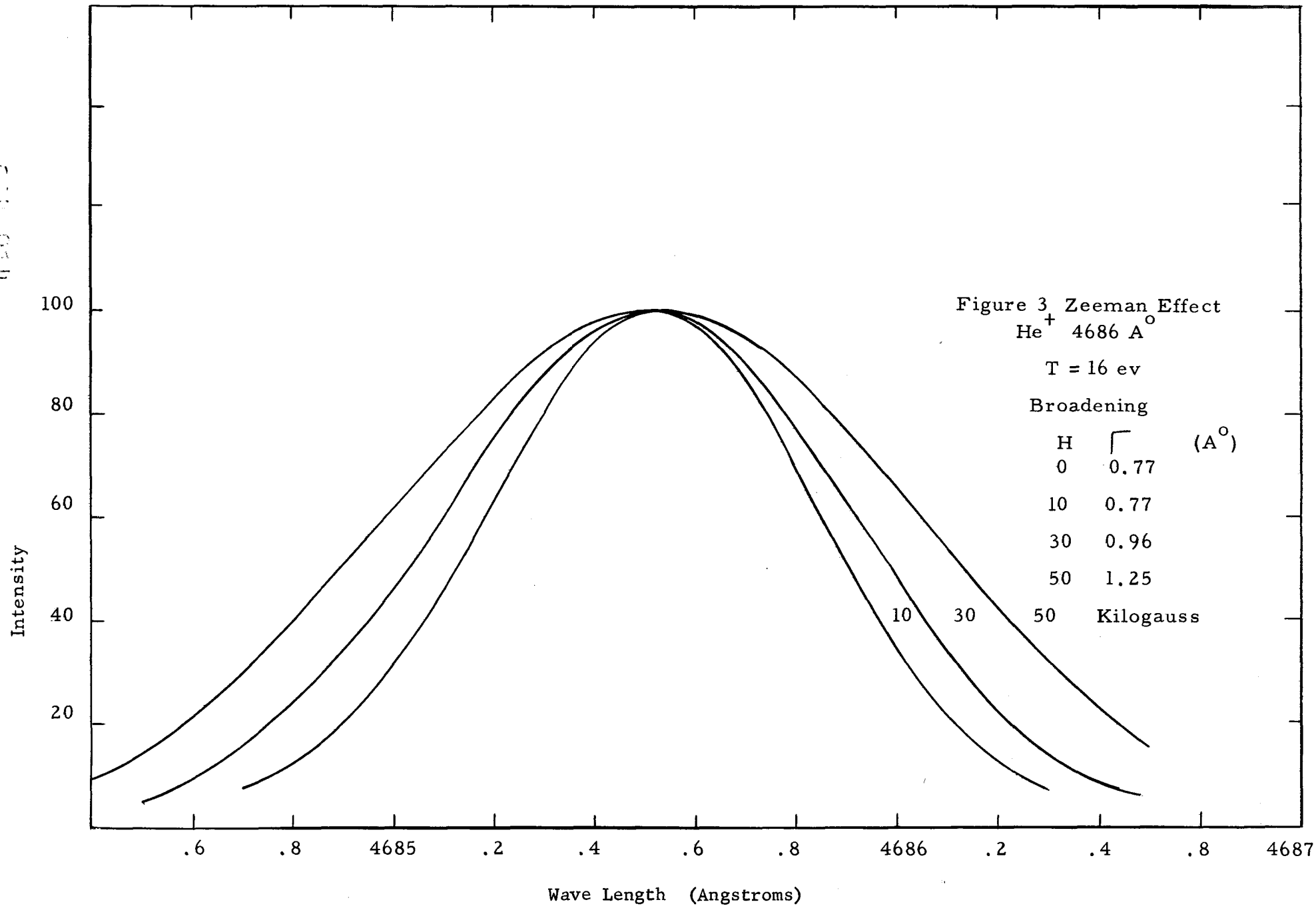

Figure 3 Zeeman Effect
He^{+} 4686 A^{o}

T = 16 ev

Broadening

H	Γ (A^{o})
0	0.77
10	0.77
30	0.96
50	1.25

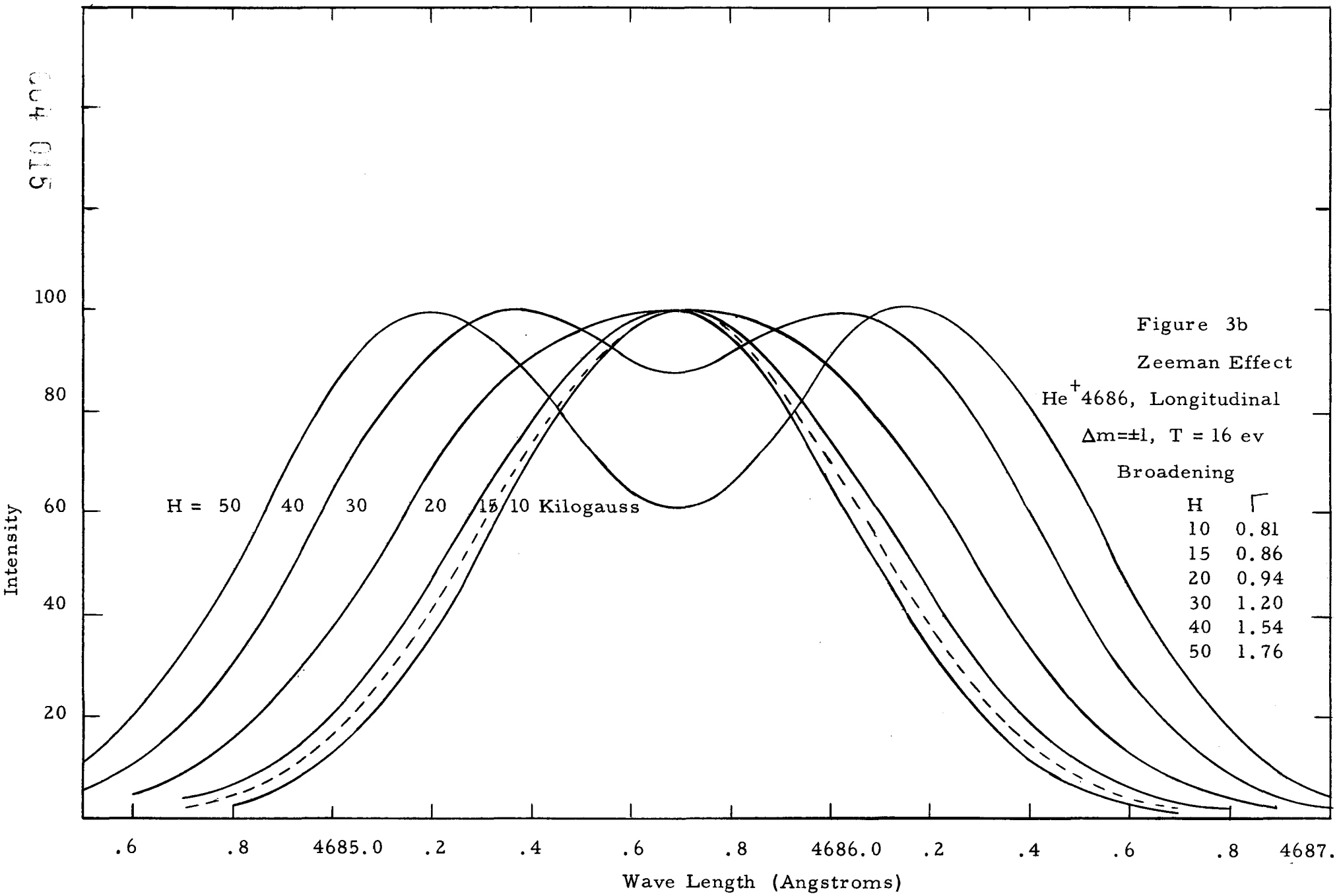
100
80
60
40
20
Intensity
H = 50 40 30 20 15 10 Kilogauss
.6 .8 4685.0 .2 .4 .6 .8 4686.0 .2 .4 .6 .8 4687.0
Wave Length (Angstroms)
Figure 3b
Zeeman Effect
He+ 4686, Longitudinal
Δm=±1, T = 16 ev
Broadening
H ⌜
10 0.81
15 0.86
20 0.94
30 1.20
40 1.54
50 1.76

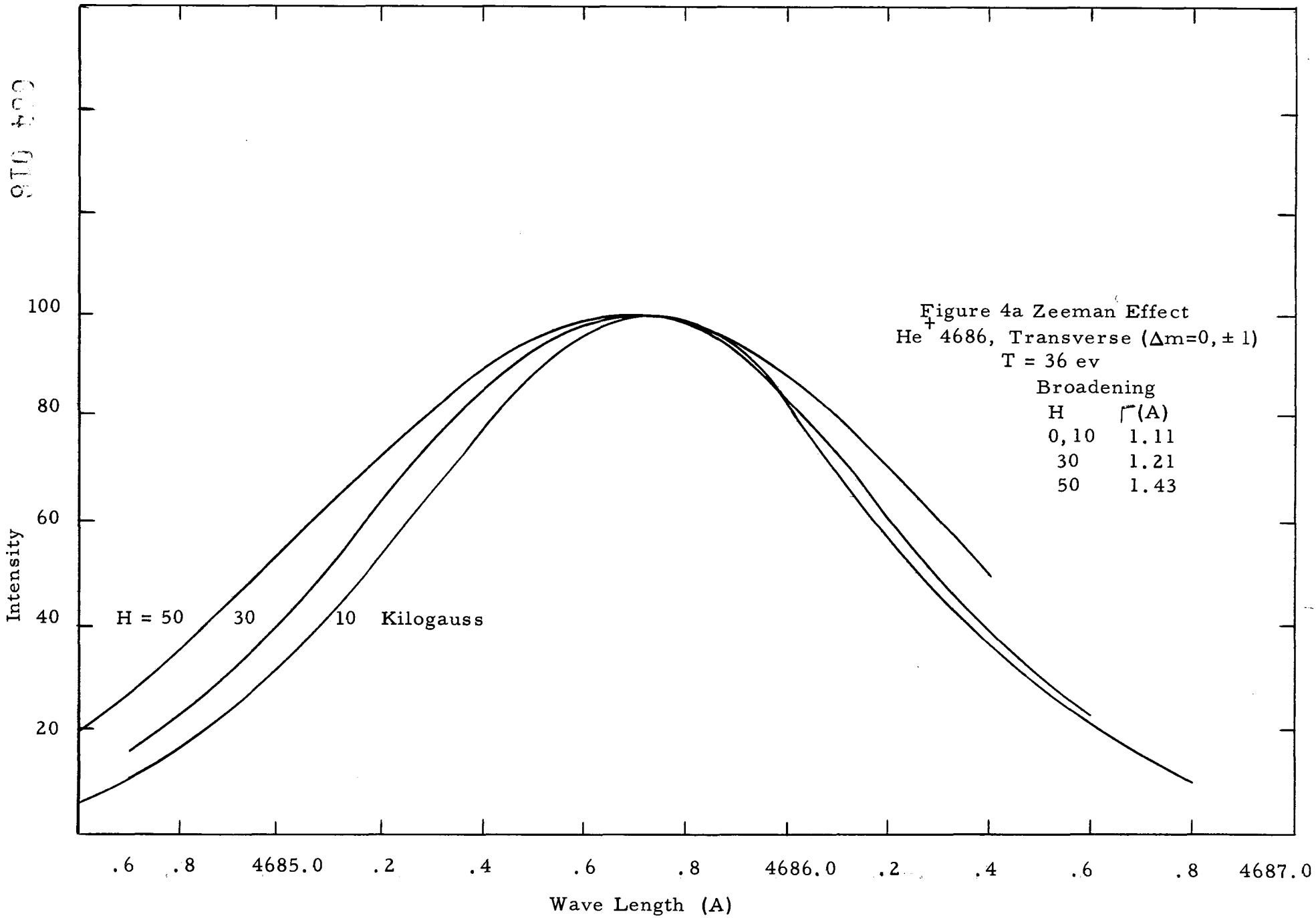

Figure 4a Zeeman Effect
He^{+} 4686, Transverse ($\Delta m=0, \pm 1$)
T = 36 ev

Broadening H	Γ(A)
0, 10	1.11
30	1.21
50	1.43

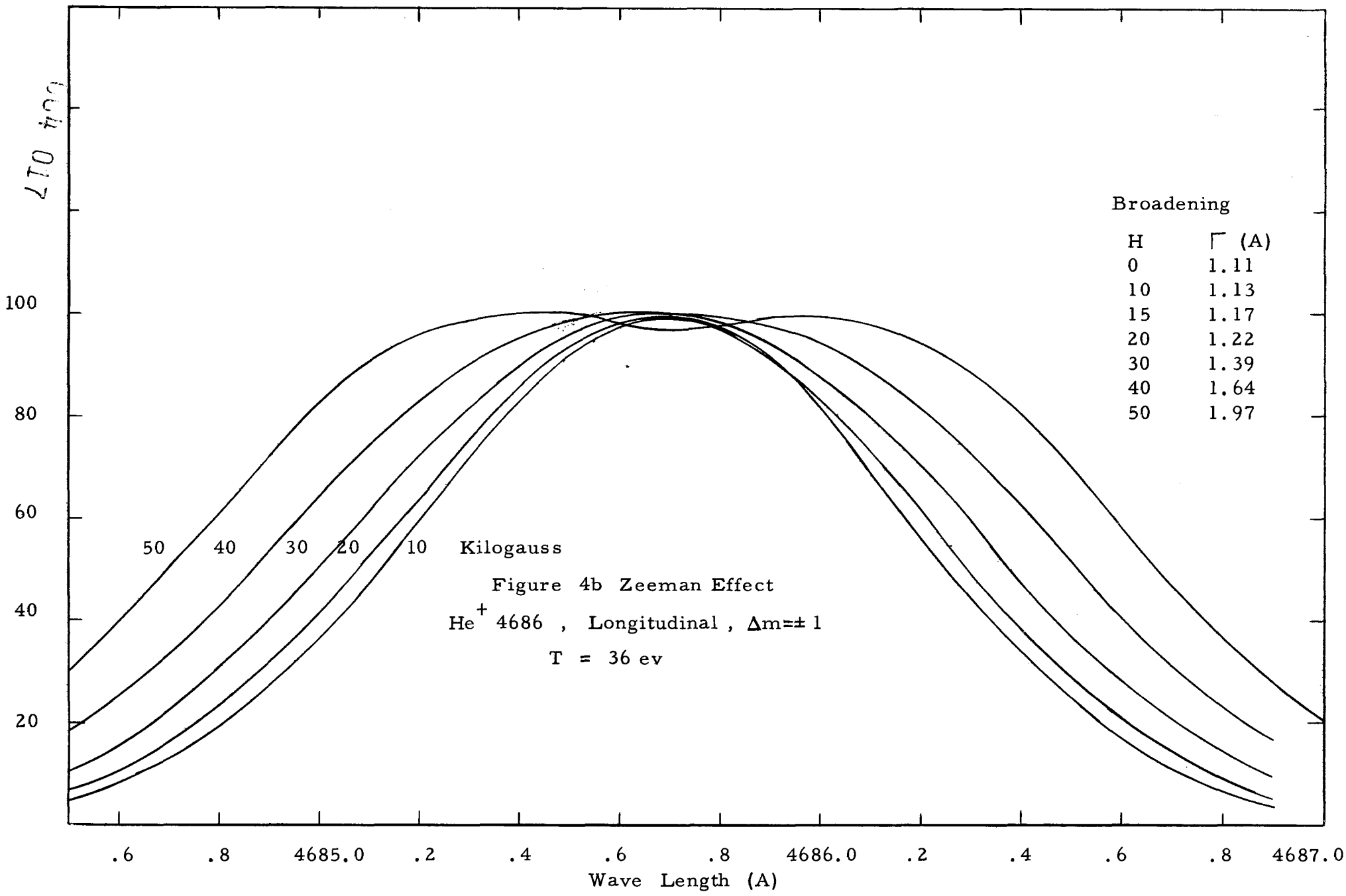

Figure 4b Zeeman Effect

He^{+} 4686 , Longitudinal , $\Delta m = \pm 1$

T = 36 ev

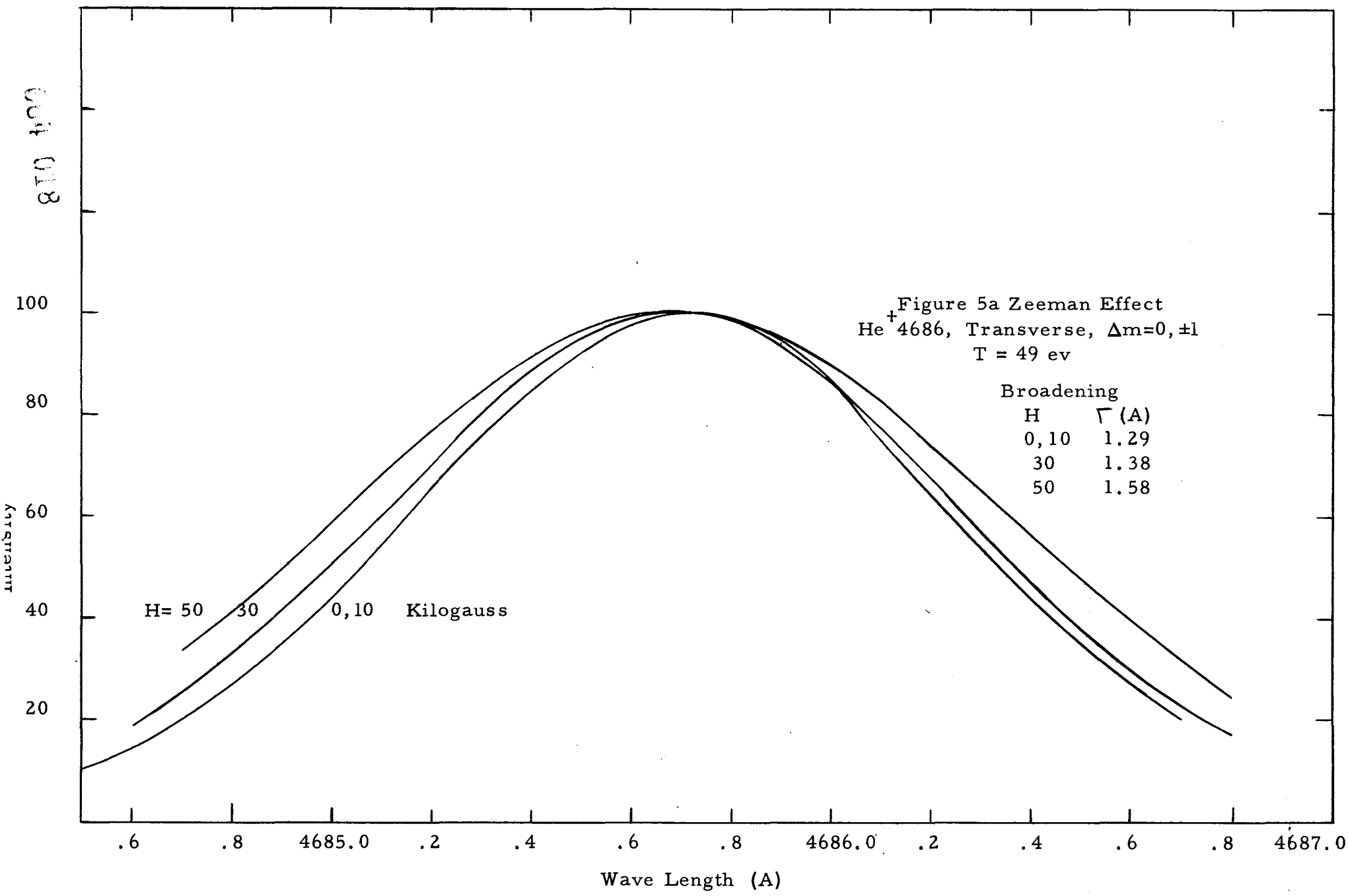
Figure 5a Zeeman Effect
He+ 4686, Transverse, Δm=0, ±1
T = 49 ev
Broadening
H Γ (A)
0, 10 1.29
30 1.38
50 1.58
H= 50 30 0, 10 Kilogauss
Intensity
100
80
60
40
20
.6 .8 4685.0 .2 .4 .6 .8 4686.0 .2 .4 .6 .8 4687.0
Wave Length (A)

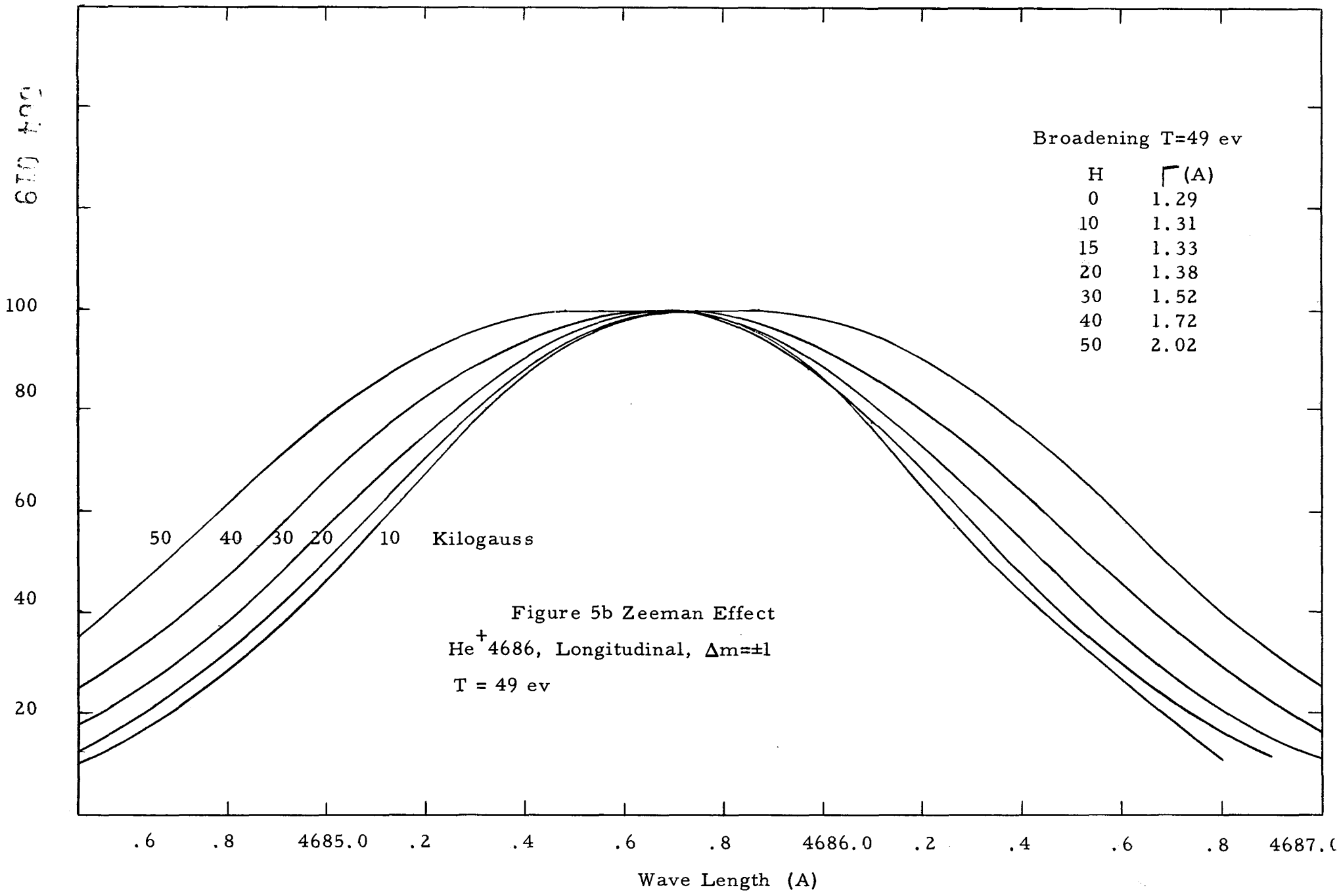

Figure 5b Zeeman Effect

He^{+} 4686, Longitudinal, $\Delta m = \pm 1$

T = 49 ev

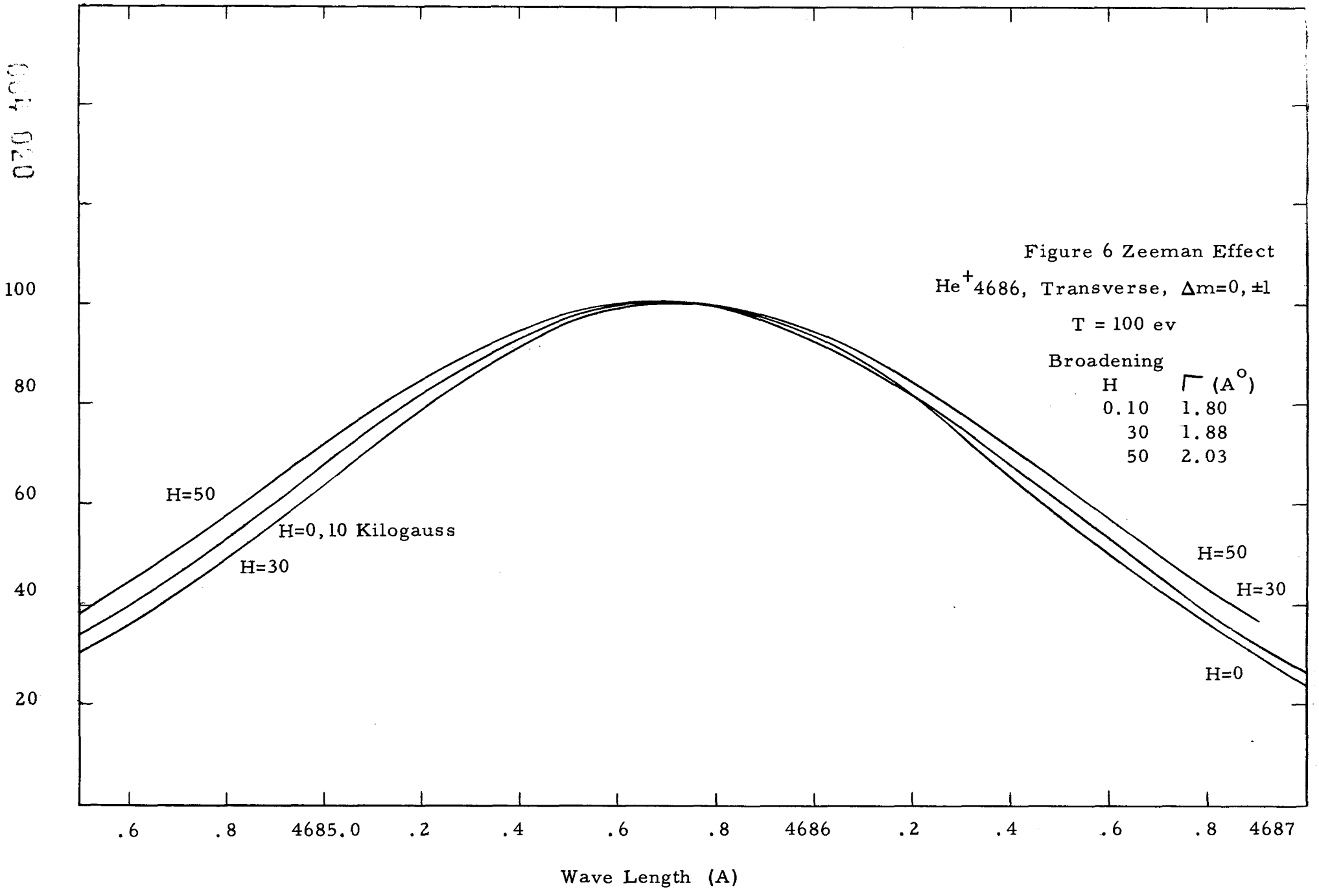

Figure 6 Zeeman Effect

He^{+} 4686, Transverse, $\Delta m=0, \pm 1$

T = 100 ev

Broadening

H	Γ (A°)
0.10	1.80
30	1.88
50	2.03

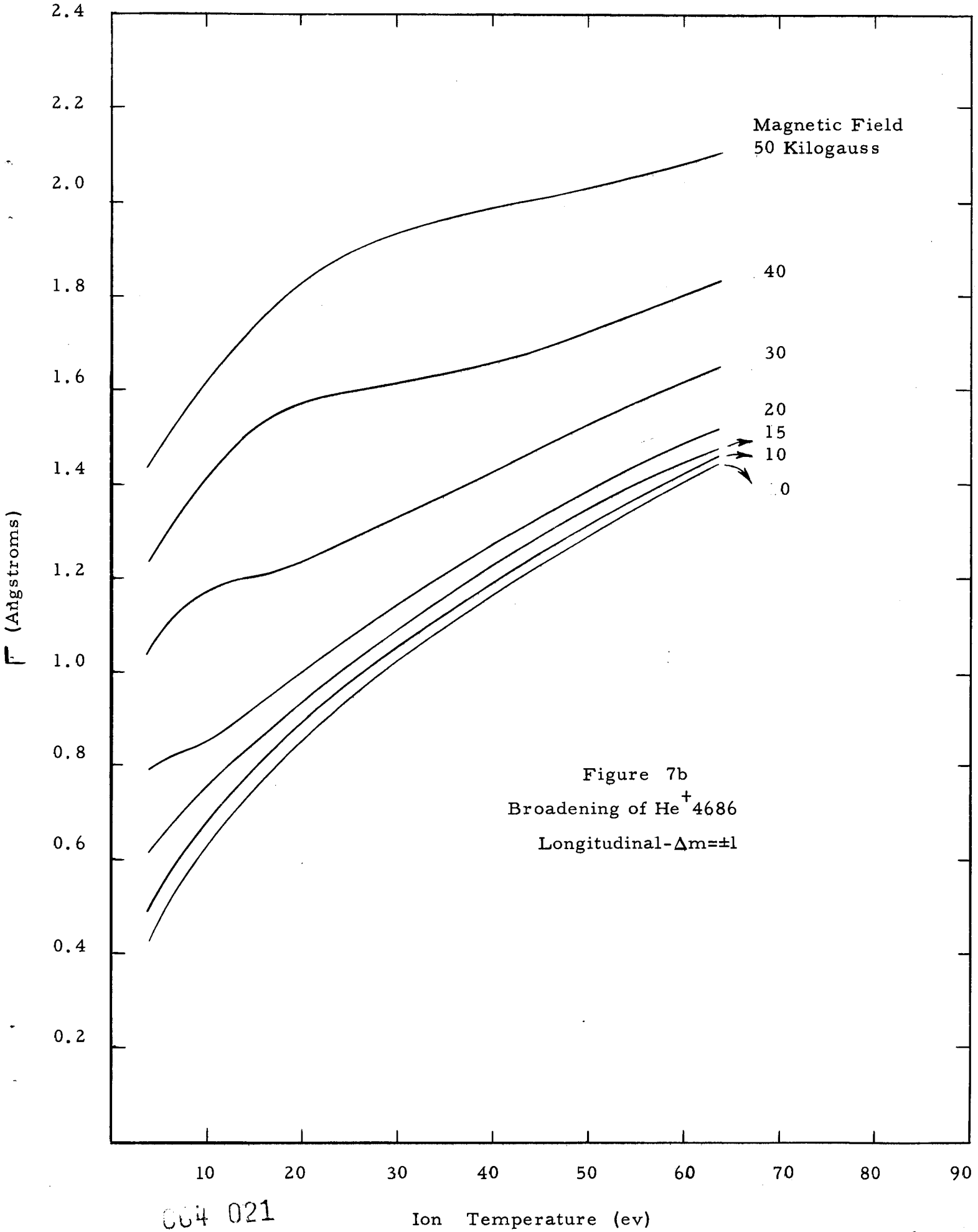

Figure 7b

Broadening of He^{+} 4686

Longitudinal-$\Delta m = \pm 1$

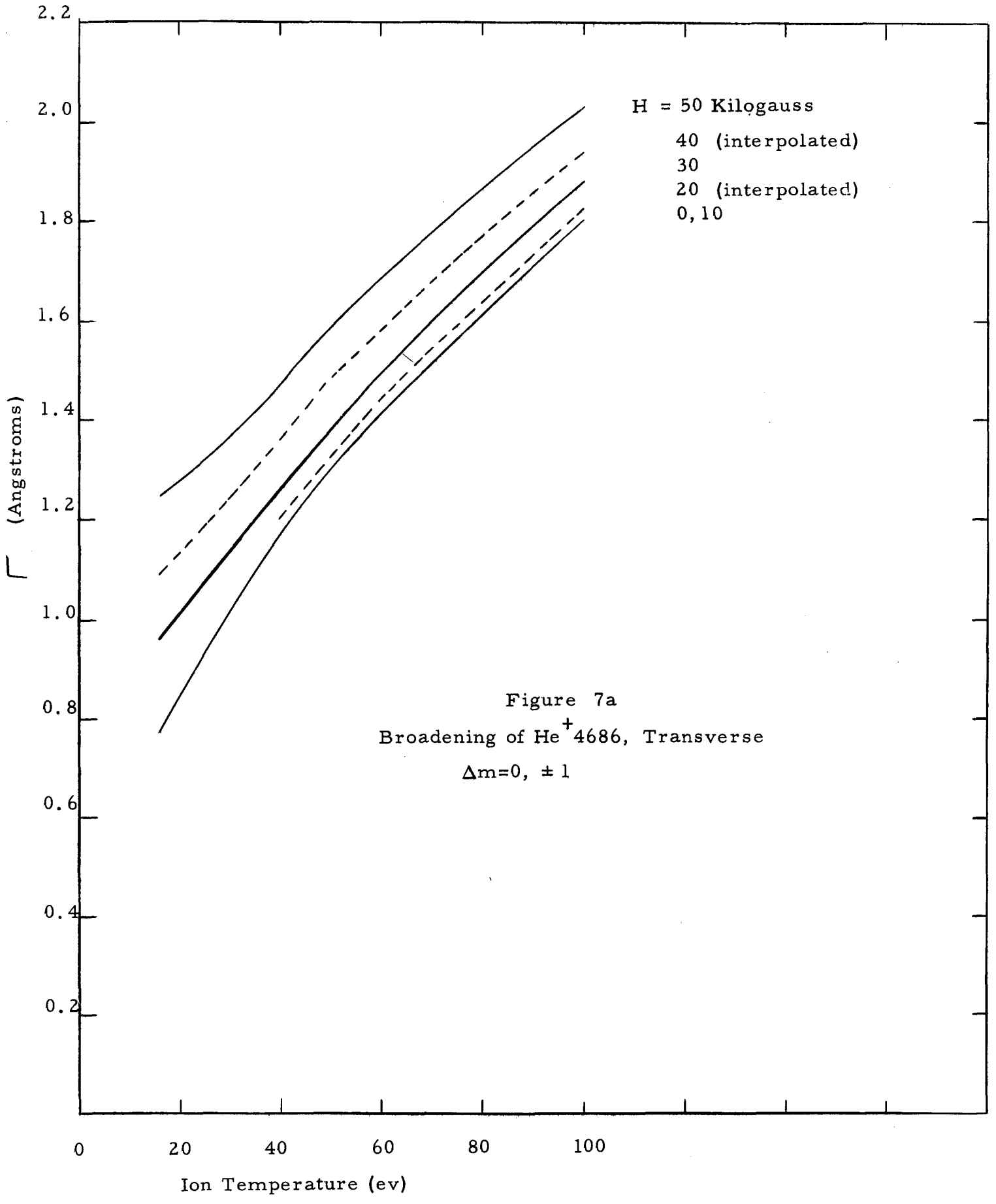

Figure 7a

Broadening of He^{+} 4686, Transverse

$\Delta m = 0, \pm 1$

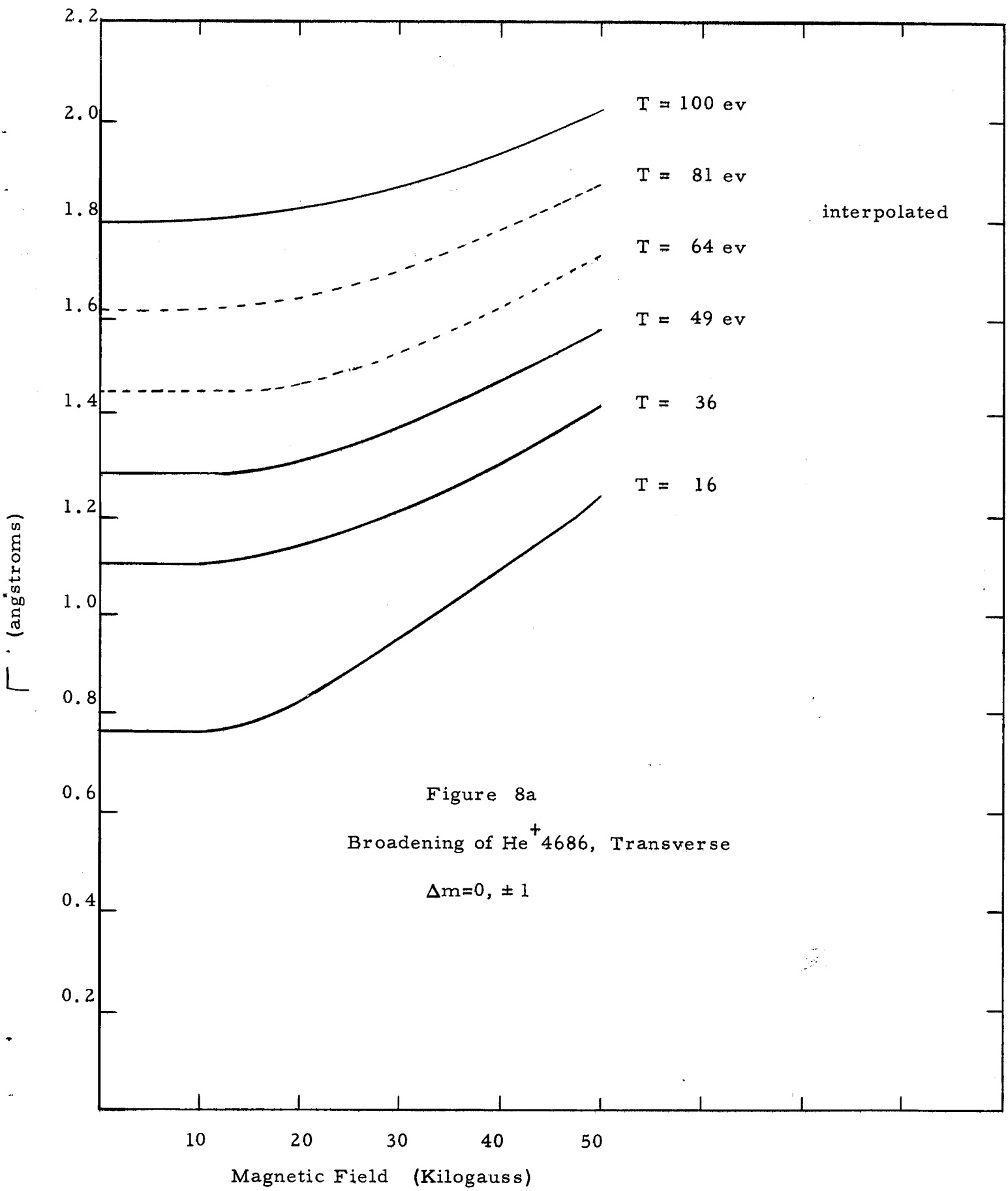

Figure 8a

Broadening of He^{+} 4686, Transverse

$\Delta m=0, \pm 1$

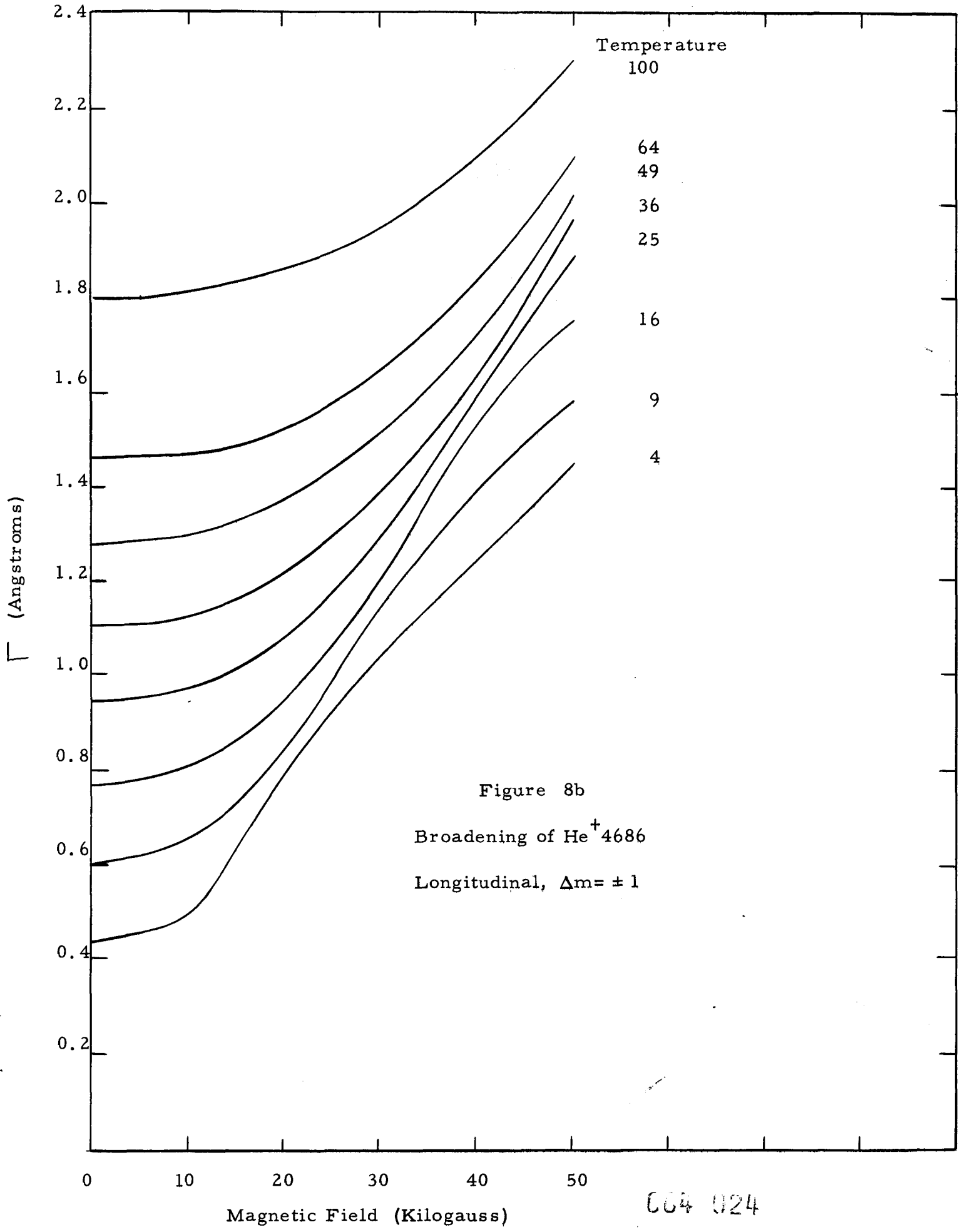

Figure 8b

Broadening of He^{+}4686

Longitudinal, $\Delta m = \pm 1$

C64 024

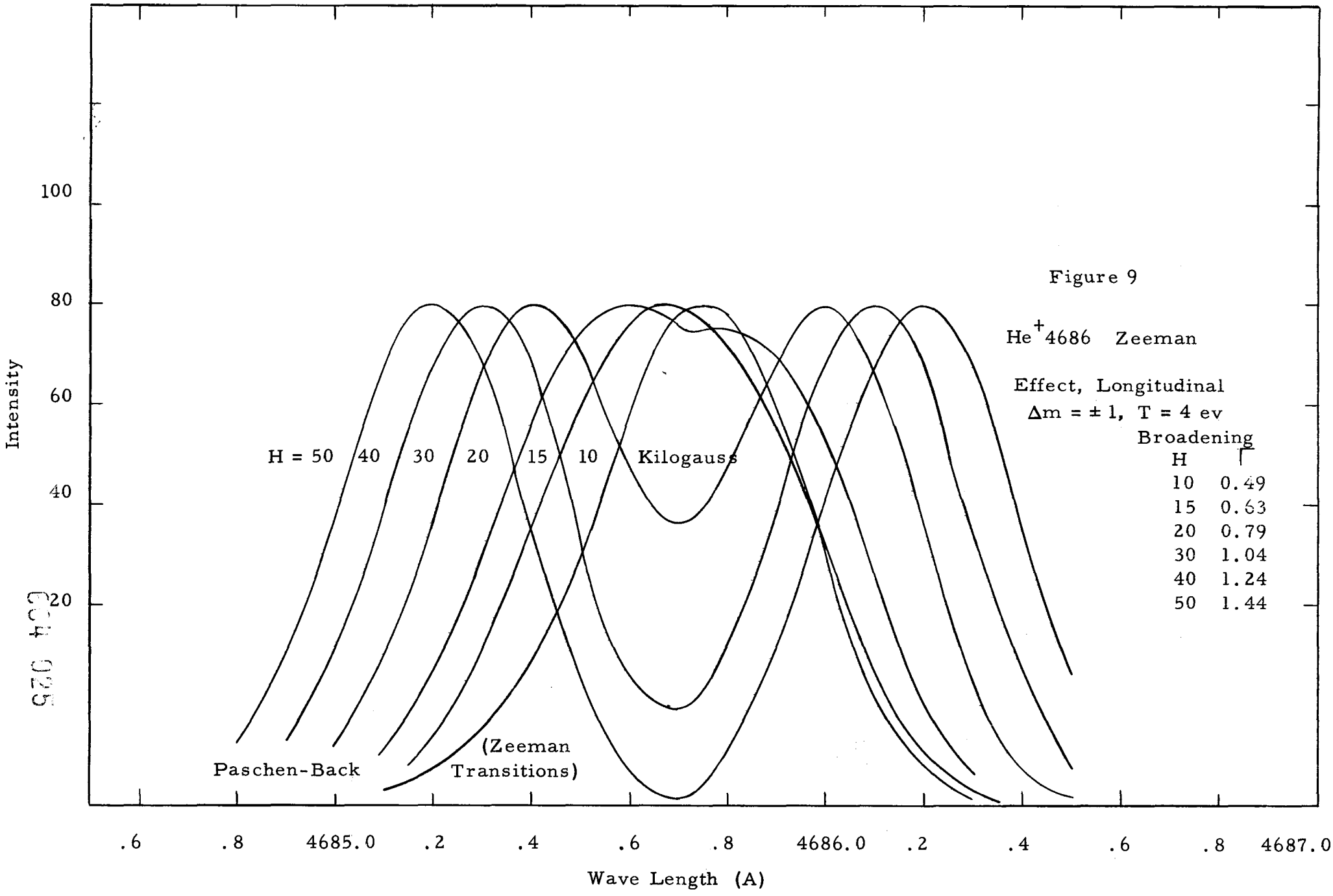

Figure 9

He^{+} 4686 Zeeman

Effect, Longitudinal

$\Delta m = \pm 1$, T = 4 ev

H	Broadening
10	0.49
15	0.63
20	0.79
30	1.04
40	1.24
50	1.44

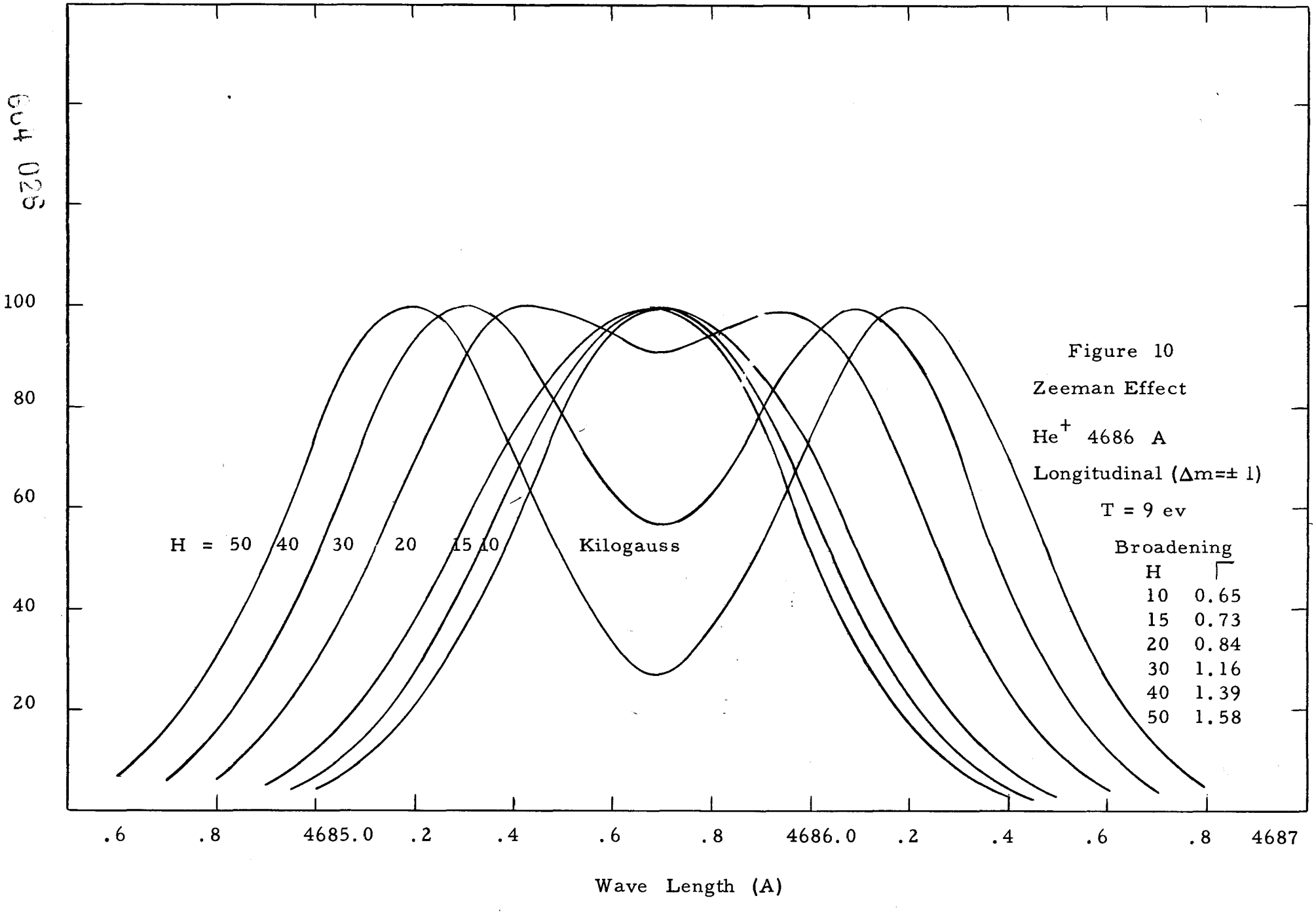
100
80
60
40
20
H = 50 40 30 20 15 10 Kilogauss
.6 .8 4685.0 .2 .4 .6 .8 4686.0 .2 .4 .6 .8 4687
Wave Length (A)
Figure 10
Zeeman Effect
He+ 4686 A
Longitudinal (Δm=± 1)
T = 9 ev
Broadening
H
10 0.65
15 0.73
20 0.84
30 1.16
40 1.39
50 1.58